Modelling daily soil salinity dynamics in response to agricultural and environmental changes in coastal Bangladesh

Andrés Payo[1, †], Attila N. Lázár[1], Derek Clarke[1], Robert J. Nicholls[1], Lucy Bricheno[2], Salehin Mashfiqus[3], Anisul Haque[3]

[1]Faculty of Engineering and the Environment, Southampton University, Southampton, SO17 1BJ, UK

[2]National Oceanography Centre, Liverpool L3 5DA, United Kingdom

[3]Bangladesh University of Engineering and Technology, Dhaka-1000, Bangladesh

[†]British Geological Survey, Keyworth, NG12 5GD, UK (current address)

Corresponding author: Andrés Payo (agarcia@bgs.ac.uk)

Key Points:

- A novel 'regional' soil salinity model is developed to assess long term (days to decades) changes in coastal lowlands and applied in coastal Bangladesh.
- This model can reproduce the soil salinity time series under multiple land uses, including rice crops, combined shrimp and rice farming, as well as non-rice crops.
- Results indicate a moderate increase in soil salinity to 2050 that can potentially cause significant crop yield reductions, especially for vegetables and local rice varieties.

Abstract

Understanding the dynamics of salt movement in the soil is a prerequisite for devising appropriate management strategies for land productivity of coastal regions, especially low lying delta regions which support many millions of farmers around the world. In this research, we develop a novel holistic approach to simulate soil salinization comprising an emulator-based soil salt and water balance calculated at daily time steps. The method is demonstrated for the agriculture areas of Coastal Bangladesh. This shows that we can reproduce the dynamics of soil salinity under multiple land uses, including rice crops, combined shrimp and rice farming, as well as non-rice crops. The model also reproduced well the observed spatial soil salinity for the year 2009. Using this approach, we have projected the soil salinity for three different climate ensembles, including relative sea-level rise for the period 2041-2050. The results indicate an increase in soil salinity in 21-44% of the simulated area. This can potentially cause significant crop yield reductions, especially for vegetables and local rice varieties. The modelling approach will enable planners and land use managers to investigate future trajectories of salinity impacts on crop production, considering expected changes in relative sea level, groundwater pumping and water quality in the rivers and estuary, and management responses to augment freshwater supplies.

1 Introduction

The coastal zone comprises only 3% of the earth's surface and accommodate 60% of the world's population, a figure set to increase to 80% by 2050 [*Hyun et al.*, 2009]. Worldwide, about 600 million people currently inhabit low-elevation coastal zones that will be affected by progressive salinization [*Dasgupta et al.*, 2015]. Soil salinity is a major, and the most persistent, threat to irrigated agriculture many deltas, such as in coastal Bangladesh [*D. Clarke et al.*, 2015]. In saline soils, crop growth is hampered by salt accumulation in the crop root zone. If the upward salt movement caused by evaporation exceeds the downward gravitational movement, salt will accumulate in the root zone. Salt in the soil interferes with the crop growth when its concentration exceeds the tolerance limits of the crop [*Ayers and Westcot*, 1985; *Rhoades and Merrill*, 1975]. Most plants suffer salt damage at salinities equivalent to electrical conductivity of the soil saturation extract (ECe) of 4 dS/m or higher. Plant growth is restricted even though enough water may be present in the root zone, because salt reduces the plant's ability to take up water and can also be toxic to the plant. In Bangladesh, >30% of the net cultivable land is in the coastal area. Of the 1.689 Mha of coastal lands, about 1.056 Mha are adversely affected by varying degrees of soil salinity [*SRDI*, 2010]. The agricultural sector of Bangladesh constitutes an important component of the national economy accounting for around 21% of the national GDP. It also employs a significant proportion of the 35 million people (25.7%) who inhabit the coastal zone. For these people, the growth and sustainability of the agricultural sector is of paramount importance to their own prosperity and survival, as well as the national economy. Even though there is ongoing research and development to create salt and drought tolerant crop varieties, expected future sea level rise, climate variability and extremes such as cyclones and storm surges, pose a real threat to livelihoods and food security in coastal Bangladesh [*GED*, 2009]. *Lazar et al.* [2015] show that climatic change alone is unlikely to reduce agricultural productivity in southern Bangladesh, but salinity is a significant problem that is difficult to assess due to the multiple interacting drivers. Understanding the dynamics of salt movement in

the soil at the entire coastal Bangladesh is a prerequisite for devising appropriate management strategies to maintain and improve land productivity of coastal regions.

A recent attempt to model soil salinity for the entire coastal Bangladesh has been presented by *Dasgupta et al.* [2015] which developed an empirical multi-regression model using monthly averaged observations and projected soil salinity by 2050 in 69 districts of coastal Bangladesh. This suggests that many areas will have significant increases in soil salinity. While the study by *Dasgupta et al.* [2015] improves our understanding of salinity changes in Bangladesh's agricultural soils, it is a data driven approach and therefore constraint by the frequency and spatial distribution of the observation points and assumes no changes on the land uses. Models based on one dimensional salt and water balances that include changes in land uses exits but are limited to farm size simulations or does not include the mix of crops and shrimps and fish aquaculture, or important sources of salinity such as overpotting. For example,*Oosterbaan* [2002] computes soil salt and water balances in four seasons in a year at farm scale and does not include the salt flux from flooding or mixed agriculture and aquaculture. The catchment water and salt balance model of *Bari and Smettem* [2006] and the polder model of *de Louw et al.* [2011] resolves the daily salt dynamic at regional scale (> 1000 km^2) and polder scale respectively but are limited to the stream salinity (i.e. salinity at the catchment/polder water surface network) instead of soil salinity at root zone.

Our aim is to develop a quantitative framework able to simulate daily salinity changes in the soil, taking account all the important sources and sinks of salt across a low-lying delta (Figure 1), at the scale of O(10000km^2) including changes agriculture/aquaculture practices and crop types. We demonstrate the proposed framework by applying it to a region of coastal Bangladesh O(19000km^2). The main contribution of this manuscript is on model integration and model structure validation. Establishing the validity of the structure of any system dynamic model is the first logical validation (i.e. before the accuracy testing) [*Barlas*, 1996]. We present for first time the use of emulators to resolve the water and salt balance equations at the root zone and at regional scale. Emulators are approximation models of an experiment or a more complex numerical models or simulators [i.e. *Tokmakian et al.*, 2012]. Emulators are primarily used for their speed and flexibility to represent any system. If the approximation of the system is acceptable, and if the inputs are expected to stay within the limits of the training dataset,

emulators can be used both for prediction. The analysis of which water and salt fluxes are the key drivers on the soil salinity in coastal Bangladesh are outside the scope of this work.

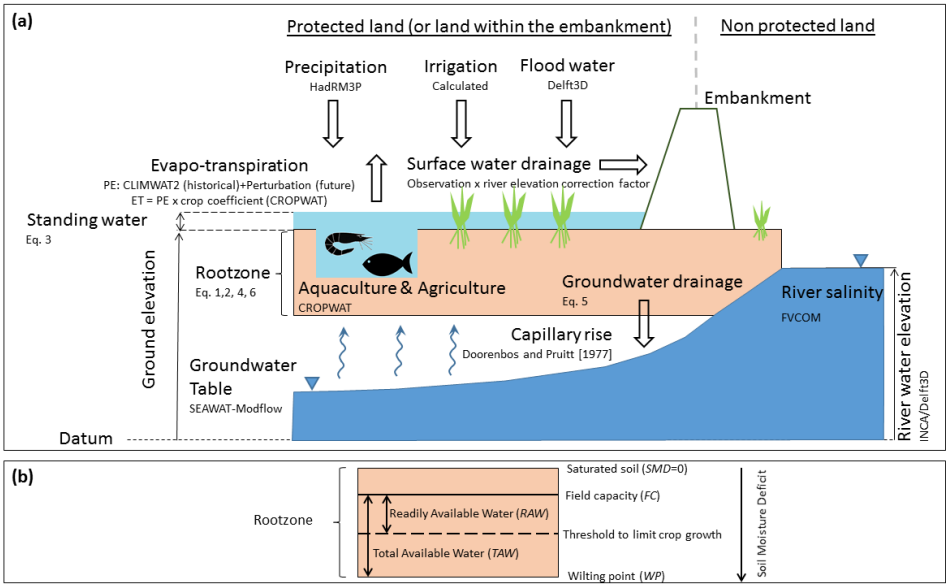

Figure 1. Soil salinity model conceptual framework: (a) main fluxes of water and salt; and (b) definition of soil moisture deficit at the root zone.

This manuscript describes the integrated soil water and salinity model and its components (Figure 1), including validation against existing soil salinity temporal and spatial observations. Firstly, the study region of Coastal Bangladesh is described. Secondly, the method used to calculate the daily soil moisture deficit (SMD) and soil salt mass balance is presented in detail: (1) the main equation that this model solves is the salt balance at the root zone but, to solve this equation we need to estimate the salt and water flux from ground water due to capillary rise (2), the inter-dependent daily water balance at soil surface (3) and root zone (4) and the salinity of the standing water (5). To solve this set of equations across coastal Bangladesh, we need a good representation of ground water depth and ground water salinity and water and salt fluxes from river and coastal flooding. Process-based models such as Delft3D [*Roelvink*, 2011], FVCOM [*Chen et al.*, 2006; *Chen et al.*, 2003] and SEAWAT-MODFLOW [*Langevin et al.*, 2003] provide a good representation at the scale of this study but are too demanding computationally to be run for decadal and longer time scales. Hence, we explore the use of emulators as a way to simulate efficiently the groundwater and estuarine hydrodynamics. The proposed method is then validated against temporal and spatial soil salinity observations. Using the validated model, soil

salinity is projected to 2050 for different climate scenarios for the south-west coastal zone of Bangladesh.

2 Materials and Methods

2.1 Description of the study site

This study comprises the south-west coastal zone - where there is a tidal influence - of Bangladesh [*Nicholls et al.*, 2016]. The study area is 18,850 km^2 (Figure 2), having about 14 million inhabitants with an average population density of 750 people/km^2. Administratively the area comprises three districts from the Khulna Division (Satkhira, Khulna and Bagerhat), and all six districts of the Barisal Division. The nine districts contain 70 upazilas (i.e. sub-district administrative units, average size: 264 km^2) and 653 unions (i.e. the smallest planning unit in Bangladesh incorporating a few villages, average size: 28 km^2, average population: 21,800) within the study area.

This area is low-lying: the land elevation ranges from one to three metres above sea level, but most of the study area is poldered (i.e. enclosed by embankments to protect the area from floods and salinity intrusion). The tidal range varies between 0.5 and 4.5 metres. The land cover in 2010 was dominated by agriculture (45%), followed by natural vegetation (12%), aquaculture (11%), water (8%) and wetland (8%). This deltaic region provides a range of important ecosystem services which make it highly suitable for agriculture which provides livelihoods for most of the coastal population. The delta plain of the Ganges–Brahmaputra–Meghna river system supports numerous ecosystem services and livelihoods [*Nicholls et al.*, 2016]. About 85 percent of the people of the coastal zone are partially or wholly engaged on agriculture. Because of the high population density, over 50 percent of the households are practically landless having less than 0.2 hectares of land. Fishing, crop agriculture, shrimp farming and tourism are the area's main economic activities.

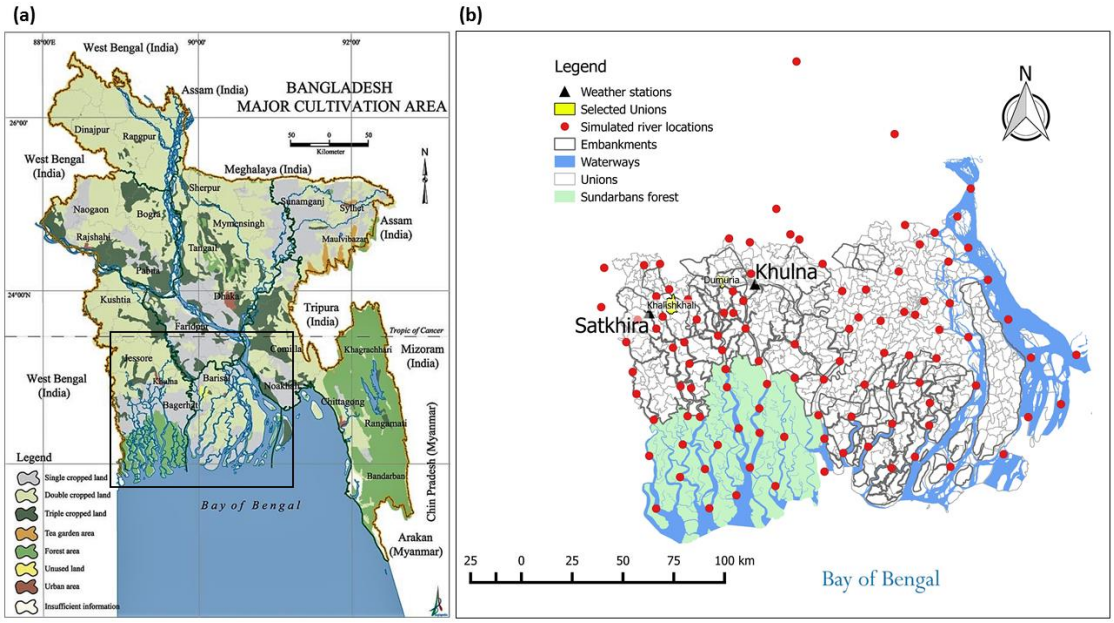

Figure 2. Study zone is located in South-Western side of coastal Bangladesh. (a) Most land is single or double cropped land (source Banglapedia). (b) Unions, embankments and locations of the weather stations and simulated river locations within the study zone.

There are three distinct seasons in Bangladesh agriculture: Rabi season (November–March; cool, dry winter), Kharif-1 season (March–June; hot humid summer) and Kharif-2 season (June–November; monsoon). In the 1990s, farms practiced mono cropping (i.e. having only one season crop), but wherever irrigation water is available, crops have been recently started to be cultivated in two and three cycles per year. Multi-cropping has become more common because of a higher awareness of alternative crops due to agricultural extension services and non-governmental organisation (NGO) interventions. Additionally, a higher availability of irrigation water, through the installation of diesel-driven tube-wells funded by NGO loans has enabled the capital investment required for high yielding varieties (HYVs). The traditional crop is rice (varieties are Boro, Aus, Aman, cultivated generally in the Rabi, Kharif-1 and Kharif-2 seasons, respectively), but cash-crop production is increasing and includes crops such as wheat, chilli, potato, mustard, tomato and grass pea. Furthermore, because of agricultural research and development projects, the traditional local varieties of crops have been almost completely replaced by more resilient hybrid and HYVs.

The highest average maximum temperature in the study area is 33^{o} C and above during March to May, and the lowest average minimum temperature is about 15^{o} C in December and January. The south-western region of Bangladesh receives an average rainfall of about 1730 mm per annum, of which about 78 percent falls within the 4 months of the monsoon. Monsoon rains are important for both providing soil moisture and irrigation water, and flushing the salinity from the soils. However, soil salinity is more spatially variable due to localised environmental processes and management practices (e.g. irrigation, polderisation, etc.). Precipitation generally

increases from west (~1700 mm/year) to east (~2600 mm/year) in the study area, although there is smaller north (2300 mm/year) to south (2600 mm/year) gradients.

2.2 Soil moisture deficit and soil salinity governing equations

SMD is defined as the amount of water in units of mm of rain (or irrigation) required to re-wet a dry soil so that the plant root zone is at field capacity (i.e. it can hold no more water). The SMD and salt balance model is based on the FAO CROPWAT single layer approach [*D Clarke et al.*, 1998] and the salt balance mass equations [*D. Clarke et al.*, 2015]. It requires many parameters including daily values of rainfall and temperature, potential evapotranspiration, crop characteristics (cropping pattern calendar and area cover, crop type, rooting depth and crop coefficient), soil characteristics (soil type, structure and porosity), ground elevation, and daily water and salt fluxes due to river and coastal flooding, capillary rise and irrigation. The scale of analysis here is the union level. Daily soil salinity time series are calculated for each one of the 653 unions and for each crop type. Soil salinity for a given cropping pattern –a set of crop types- is calculated as an area averaged value. Water and salt fluxes can be significantly different for crops being grown in the land within the embankments –protected land- than in the non-protected land leading to different soil salinity time series (e.g. char land is frequently flooded adding salt from the river or brackish water). The union-protected land area is calculated as the union area that is within any of the existing embankments and the remaining union area is assumed to be non-protected. Crop soil salinity time series are calculated for the protected and non-protected land and, the results are area averaged to produce a unique union specific soil

190 salinity time series. The SMD and salt mass balance equations and the source of all the other
191 input parameters are discussed below.

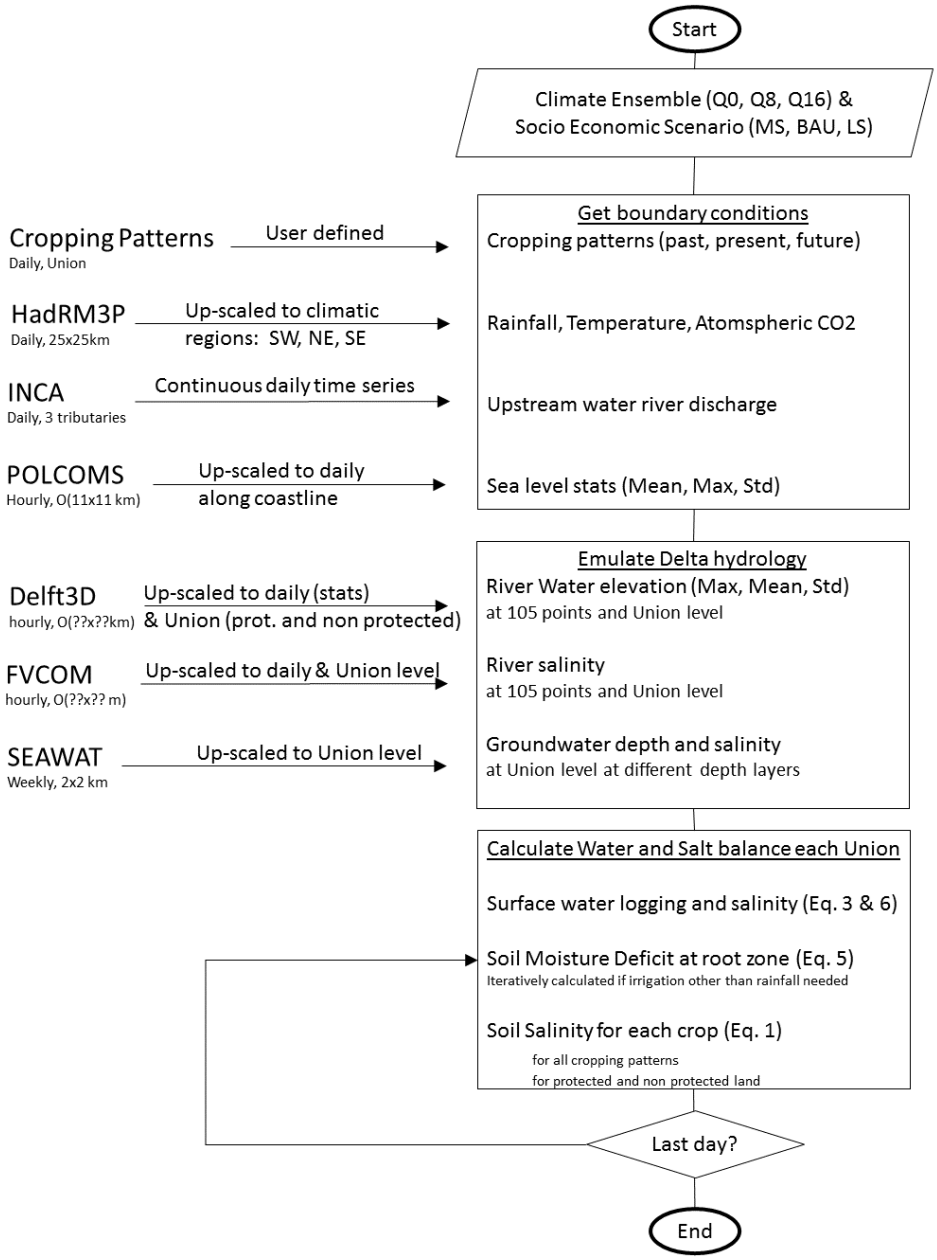

192

193 **Figure 3**. Flow chart of the proposed integrated soil salinity model.

194

195 2.2.1 Main governing equation: daily salt mass balance in the root zone

196 The salt balance at the root zone, which extends from the land surface to the crop-specific
197 maximum root depth, is basically a statement of the law of conservation of mass. In its simplest
198 non-stationary form, it is:

$$y_{rz,t} = y_{rz,t-1} + IC_i + GC_g + IrrC_{irr} - RC_{rz} \quad (1)$$

where $y_{rz,t} =$ is the salt mass content in (gr) at the root zone at a given time (t) and $y_{rz,t-1}$ is the salt mass content at the previous time step; IC_i is the net salt flux due to infiltration from land surface (I being the surface water infiltration rate (mm/day) and C_i being the salt concentration of infiltrated water (gr/l)); GC_g is the net salt flux due to capillary rise from ground water (G being the water capillary rise rate (mm/day) and C_g being the salt concentration of ground water (gr/l)); $IrrC_{irr}$ is the net salt flux due to irrigation, being Irr is the irrigation rate (mm/day) and C_{irr} is the salt concentration of irrigation water (gr/l); and RC_{rz} is the net salt out flux due to percolation, being R the water percolation rate (mm/day) and C_{rz} is the salt concentration at the root zone (gr/l). To obtain this simple salt balance equation, we make the following assumptions:

- All salts are highly soluble and do not precipitate;
- The amount of salts supplied by rainfall is negligible;
- The amount of salts supplied by fertilizers and exported by crops are negligible.

We can regard the amount of salt at any given time in the root zone ($y_{rz,t}$) as being dissolved in the soil water. Because the downward movements of water and salt generally take place at water contents near field capacity, we can logically consider y_t to be dissolved in an amount of water $W_{rz,fc}$, which is the amount of soil water at field capacity expressed in mm. $W_{rz,fc}$ can be determined from:

$$W_{rz,fc} = \theta D \quad (2)$$

where θ is the soil effective porosity (typically 0.12 for the silty clay soils of coastal Bangladesh) and D is the depth of the root zone (mm). For the sake of simplicity, the depth of the root zone is defined for each crop type as the maximum depth at the end of the development stage. The salt concentration in the root zone is then defined as $C_{rz} = y_{rz,t}/W_{rz,fc}$ and equation (1) can be now iteratively solved if all the salt and water fluxes (Fig 1) and the initial soil salt content at the root zone are known. To avoid negative soil salinities when solving Eq. (1) the salt removed by percolation at each time step is obtained as the minimum between the amount of salt before percolation ($y_{t-1} + IC_i + CRC_g$) and the salt carrying capacity(RC_r). If the salt carrying capacity due to percolation is smaller than the amount of salt in the soil some will remain and *vice versa*.

2.2.2 Salt and water flux from ground water due to capillary rise

In irrigated areas, during intervals in irrigation or during fallow periods when there is no downward flow or percolation water, water can move upward by capillary forces. The water will be taken up by the roots or evaporate at the surface and salt will accumulate in the root zone or in the soil top layer. The capillary upward flux varies with soil type, depth of water table, and soil water gradient [*Ritzema*, 1994]. Most top soil in coastal Bangladesh is made of silty clay soils [*D. Clarke et al.*, 2015]. Because very detailed experiments will be required to determine the

groundwater contribution under field conditions we used the capillary rise estimates for clay soil types suggested by *Doorenbos and Pruitt* [1977]. No capillary flow occurs if the groundwater table is within the root zone or waterlogging occurs (i.e. standing water depth at soil surface is larger than 0) and the plants cannot form air ducts. The time step of one day implies that some of the calculated flow rates may result in moisture contents exceeding the total water storage capacity at the root zone, limiting the values of capillary rise rate suggested by *Doorenbos and Pruitt* [1977]. Changes in depth to groundwater due to capillary rise are assumed negligible relative to seepage from rivers and groundwater pumping.

The depth to ground water and the salinity of groundwater is obtained from an emulator trained with MODFLOW-SEAWAT simulations for the period 1981-2098 under three different climate scenarios. MODFLOW-SEAWAT is a software that simulates three-dimensional variable-density groundwater flow coupled with multi-species solute and heat transport [*Harbaugh*, 2005; *Langevin et al.*, 2003]. The SEAWAT model was set-up for a domain larger than the study region encompassing the greater southwest region in Bangladesh (Figure 4). The model uses groundwater pumping volume, general head, flow and river boundary conditions and includes all the significant rivers in the southwest coastal zone to allow for river-aquifer interaction. The model is conceptualized (and subsequently discretized) as consisting of the soil layer, the first (upper) aquifer (a composite aquifer consisting of complex patterns of very fine to medium sand), an aquitard and the second (deeper) aquifer. The model is discretized into a 2 km x 2 km grid, with 10 vertical layers in the first aquifer and 8 vertical layers in the second aquifer. This was done based on lithological analysis of nearly 2700 bore logs for the ESPA Deltas study [*Nicholls et al.*, 2016]. The main model outputs are the depth to groundwater tables (or piezometric heads) and salinities in the different layers. The SEAWAT gridded outputs are aggregated into an area averaged union time series. The simulated salinity of the first aquifer (less than 10m depth below water surface) is used to characterize the ground water salinity (C_g). The salt flux due to capillary rise is obtained as the product GC_g.

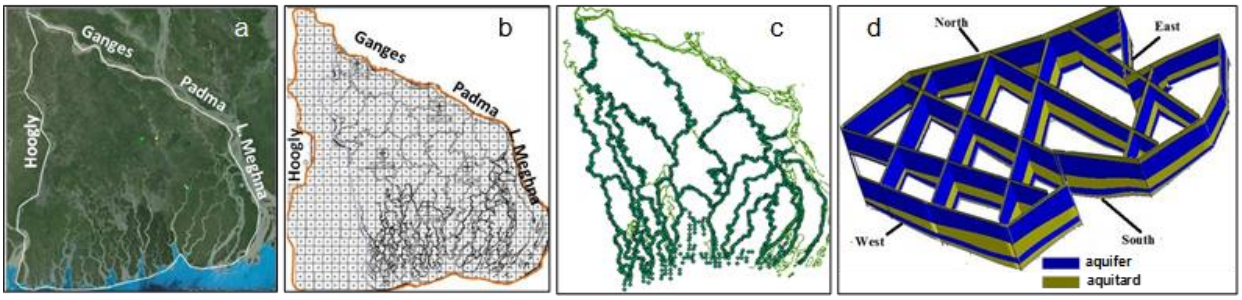

Figure 4. Simulation of depth to groundwater and ground water salinity using the MODFLOW-SEAWAT model: (a) model extent; (b) horizontal discretization; (c) rivers considered for simulation of river-aquifer interaction; and (d) stratigraphic representation of the aquifers.

268 2.2.3 Daily water balance at soil surface

269 Because the rate of infiltration (I) in Eq. (1) is the recharge into the root zone, its value is
270 related to the inflow and outflow components of the surface water balance. These components
271 are:

272 • Water that reaches the land surface from precipitation;

273 • Water that enters the water balance area by lateral surface inflow and leaves it by lateral
274 surface outflow;

275 • Water that evaporates from the land surface.

276 The daily irrigation rate is not included as a on the daily water balance at the soil surface
277 because we assume that all water surplus after irrigation is contributing to the percolation rate
278 (i.e. leaching soil salts) but not to the surface standing water. The difference between the
279 components is due to changes in surface water storage. Infiltration in the root zone can therefore
280 be expressed by equation (3):

281 $$I_t = P_t - ET_{c,t} + F_t - DR_{s,t} - \frac{\Delta W_{s,t}}{\Delta t} \quad (3)$$

282 where

283 I_t = infiltration rate for the time interval Δt (mm/d), it varies between 0 and a union
284 specific maximum infiltration rate

285 P_t = precipitation rate (mm/d)

286 $ET_{c,t}$ = evaporation from the land surface under standard conditions (mm/d)

287 F_t = lateral inflow due to flooding (mm/d)

288 $DR_{s,t}$ = lateral outflow due to surface drainage (mm/d), it varies between 0 and a union
289 and time specific maximum rate

290 $\Delta W_{s,t}$ = the change in surface water storage (mm)

291

292 Daily precipitation and temperature values for 1981–2098 were provided by a 17-
293 member ensemble of simulations of the HadRM3P (PRECIS) regional climate model developed
294 by the Met Office Hadley Centre [*Caesar et al.*, 2015]. The model is based on the HadCM3
295 global climate model and dynamically downscaled to assess regional climate variability. The
296 model runs at a 0.22º x 0.22º resolution (~25 km by 25 km), with 19 vertical levels and 4 soil
297 levels. The ensemble member (labelled Q0) represents an unperturbed version of the model
298 physics. The projections are driven by the Special Report on Emissions Scenario (SRES) A1B
299 scenario, which lies between RCP6.0 and RCP8.5 in terms of atmospheric CO_2 concentrations

and global temperature projections. This represents a future for the coastal areas in Bangladesh which is approximately 4º C warmer and 9% wetter by the year 2098. This paper considers results from the unperturbed model Q0 and two alternate scenarios to examine the sensitivity of the models developed: one which is warmer and drier (Q8) and another which is warmer and wetter (Q16) over the model domain. To eliminate extreme daily precipitation values in HadRM3P dataset, we represent this spatial distribution with three climatic regions (NW, NE and SE) by averaging the 25km x 25km grid values. NW is Khulna division, NE is the northern part of Barisal division and SE is the southern part of Barisal division.

Evaporation under standard conditions from the land surface ($ET_{c,t}$) is calculated as the product of the Potential evapotranspiration (PE) and the crop coefficient (K_c) which varies with the environmental conditions, crop type and development stage. The crop evapotranspiration under standard conditions is the evapotranspiration from disease-free, well-fertilized crops, grown in large fields, under optimum soil water conditions, and achieving full production under the given climatic conditions [*Allen et al.*, 1998]. The crop coefficient (K_c) represent the ratio of ($ET_{c,t}$) and PE. For a given crop, (K_c) varies with the stage of development. For bare soils we assume that $K_c = 0.8$ which is the lowest value recommended by *Doorenbos and Pruitt* [1977] to be used in tropical regions. The PE was estimated using the same approach followed by *D. Clarke et al.* [2015]. Using the FAO Penman Montieth approach with historical average climate data from the CLIMWAT 2 database [*Muñoz and Grieser*, 2006], daily values of PE were obtained by linear interpolation between monthly values. Inter-annual variability of PE is known to be small and only has a small impact on vegetation development [*Fatichi and Ivanov*, 2014], so the historical data were assumed to remain constant over a 20 year time period 1981–2000. Estimates of future potential evapotranspiration (PE) were generated by perturbing the historical climate data for the years 2014, 2030, 2050 and 2080 [*D. Clarke et al.*, 2015]. This approach was used in place of calculating daily PE values from HadRM3P generated climate data because the HadRM3P daily temperature and humidity sequences were generated independently and produced inconsistent sequences of PE. The main impact of climatic change is to raise the mean monthly evapotranspiration rate by approximately 0.15–0.2 mm per day by the 2080s. Annual total PE rises in this period approximately 6% from a baseline value of 1193 mm to 1263 mm.

The daily time step implies that the calculated infiltration rates may exceed the soil maximum infiltration rate. If maximum soil infiltration rate at any given time step exceeds the maximum rate, the infiltration rate is assumed equal to the maximum rate and the excess is added to the surface water storage. If there is water standing at the soil surface –water ponding-, and the calculated infiltration rate from Eq. (3) is less than maximum soil infiltration rate, the infiltration rate is increased until either the maximum is reached, or there is no more standing water at soil surface for the given time interval. The surface run-off rate for each time step is assumed to be equal to the minimum of the maximum surface drainage rate and the excess net inflow of water. If there is still a net water inflow after subtracting the infiltration and evapotranspiration out flux, the excess is assumed to be lost as surface run-off until the maximum surface run-off rate is reached. The standing water level will rise if the net water influx (precipitation, flooding) are larger than the net water out flux (infiltration, run-off, evapotranspiration). Infiltration calculations under pond aquaculture are treated slightly different. For aquaculture, ponding is assumed to be maintained while the aquaculture is active. During the pond active period, infiltration is always maximum, pond salinity is assumed equal to the optimal crop growing

344 salinity and run-off is assumed zero. When aquaculture is finished, run-off is non-zero and
345 calculated as for any other crop.

346 Most surface drainage systems in coastal Bangladesh are gravity driven and therefore the
347 maximum surface drainage rate depends on the elevation difference between the union ground
348 elevation and the nearby river elevation. The union hypsometric curves (area at a given
349 elevation) are used to assess whether there is a reduction of drainage or not. For each time step
350 the maximum drainage rate is calculated as:

351 $$DR_{smax,t} = f_R DR_{smax} \quad (4)$$

352 where $DR_{smax,t}$ = is the union specific maximum surface drainage rate (mm/d) at time t and
353 f_R = is a drainage correction factor [0, 1]. The drainage correction factor (f_R) is assumed to be
354 proportional to the area below the river elevation. If none of the union area is below the nearby
355 river elevation level, the drainage correction factor is 1 and the maximum drainage rate for this
356 time interval is equal to R_{smax}. If all union area is below the nearby river water elevation the
357 drainage correction factor is 0 and no run-off occurs for this time interval. The river water
358 elevation is defined as the weighted averaged river elevation for each union using the emulated
359 river elevation at 105 locations within the study zone. The weights are proportional to the
360 Euclidean distance between the union centroid to each simulated river station ($Ed_{c,r}$). If the
361 Euclidian distance is larger than 50km, weights are 0 and if the distance is less than 50km, the
362 weights increases as $(Ed_{c,r}/50km)^2$.

363 The lateral water inflow due to flooding is obtained from an emulator trained with
364 simulated flooding with Delft3D for a set of 14 climate scenarios and sea level scenarios (see
365 Table S2 for details on the simulated scenarios). Delft3D-flow is a hydrodynamic model which
366 describes temporal variation of flow parameters in three dimensions. The model solves the
367 unsteady mass and momentum conservation equations by using a finite difference method
368 [*Deltares*, 2011] and computes water elevation, water depth, velocity and discharge at each
369 schematised computational grid point (including land, river and sea) in the model domain. The
370 domain is bounded in the north by the major rivers of the system, i.e., the Ganges, Brahmaputra
371 and Meghna. The upstream flows are computed with the INCA model [*Whitehead et al.*, 2015].
372 The tidal water levels at the sea boundary of the Delft-3D domain is provided by the simulation
373 of the Bay of Bengal by *Kay et al.* [2015] using the Global Coastal Ocean Modelling System
374 (GCOMS). The east is bounded by the Lower Meghna River. The Delft3D-morphology model is
375 coupled with the Delft3D-flow model to include the effects of changed bathymetry due to
376 changed hydrodynamics. The time step is ten minutes. For further details about this application
377 of Deltf3D to the study area, see [*Haque and Rahman*, 2016]. Main Delft3D outputs are time
378 series of river elevation at 105 locations and gridded inundation water depth. The Delft3D
379 gridded outputs are aggregated into two different time series for the protected and non-protected
380 land within each union. For each union, the daily inundation water depth (mm) and inundation
381 area (ha) are obtained. The lateral inflow due to flooding (F_t) in mm/d is obtained as the
382 elevation difference between the day of interest and the previous day. If the elevation difference
383 is positive –inundation depth has increased- the net lateral influx is equal to the elevation

difference divided by the time interval. If the elevation difference is negative –inundation depth has decreased- there is no net lateral inflow for this day.

2.2.4 Daily water balance of the root zone and irrigation needs

If the root zone soil moisture content is above field capacity, the excess water percolates deeper into the subsoil. The percolation rate from the rooted zone can be calculated as:

$$R = \frac{W_{rz,t} - W_{rz,fc}}{\Delta t} - ET_{c,t} + G + I \quad (5)$$

Where $W_{rz,t} =$ is the soil moisture amount in the root zone at a time step *t* (mm) and $W_{rz,fc} =$ is the soil moisture at root zone at field capacity (mm), and *G* and *I* are the capillary rise rate from groundwater (mm/d) and infiltration rate from soil surface (mm/d).

Not all crops are irrigated, but for those irrigated crops, the irrigation needs (mm/day) are calculated as the difference between the readily available water (*RAW*) and the moisture content on each day. Where the soil is sufficiently wet, the soil supplies water fast enough to meet the atmospheric demand of the crop, and water uptake equals $ET_{c,t}$. As the soil water content decreases, water becomes more strongly bound to the soil matrix and is more difficult to extract. When the soil water content drops below a threshold value, soil water can no longer be transported quickly enough towards the roots to respond to the transpiration demand and the crop begins to experience stress. The fraction of the total available water (*TAW*) that a crop can extract from the root zone without suffering water stress is the readily available soil water. TAW is the amount of water that a crop can extract from its root zone, and its magnitude depends on the type of soil (effective porosity) and the rooting depth (varies with crop type and development stage). The depletion fraction is assumed to be only a function of the crop type (i.e. it does not vary with the evaporation power of the atmosphere). At every time step, the soil moisture is firstly calculated assuming no irrigation is needed. If for a given crop on a given day, if irrigation other than rainfall is needed, and the resulting soil moisture is less than the threshold (we use the RAW threshold) then the amount of water needed to raise the soil moisture level up to the field capacity is calculated. The amount of water needed to raise the soil moisture is the irrigation rate used in Eq (1). The percolation rate is then calculated again by Eq. (5) but using the modified soil moisture if irrigation have occurred.

Different irrigation sources have different salinities which has been found important factors by *D. Clarke et al.* [2015] to assess the soil salinity evolution in coastal Bangladesh. When a crop is defined as irrigated, the irrigation source can be selected among rainfall, shallow ground water, deep ground water, river water or an average of shallow groundwater and river water salinities. If rainfall is selected as irrigation source, the salinity of the irrigation water is assumed negligible in Eq. (1) and is not calculated as explained above but is an input. If ground water is selected as the preferred irrigation source, this can be from the first aquifer (~less than 10m depth) or from the second aquifer (~70 – 120m depth) from the river, or from a combination

of the river and first aquifer. The salinity of the river and groundwater is emulated from using FVCOM and SEAWAT simulations as described previously.

2.2.5 Salinity of standing water

The salinity of the standing water (C_i) is defined as $\frac{y_{s,t}}{W_{s,t}}$ the ratio between the salt mass content at soil surface ($y_{s,t}$) and the standing water level ($W_{s,t}$). The amount of salt at soil surface at each time step t is calculated as:

$$y_{s,t} = y_{s,t-1} - F_t\, RivSal - (DR_{s,t} + I_t)\frac{y_{s,t}}{W_{s,t}} \quad (6)$$

where $RivSal =$ is the salinity (gr/l or ppt) at the union-nearby river stations. The river salinity is obtained from emulated daily river salinities at the same 105 locations where river elevation is emulated. As for river elevation, a Euclidian distance average value is assigned for each union. The river salinity time series at each one of the 105 virtual stations are calculated using an emulator trained with simulated salinities using the Finite-Volume Community Ocean Model (FVCOM) [*Chen et al.*, 2006; *Chen et al.*, 2003]. FVCOM is an unstructured-grid, finite-volume, free-surface, 3-D primitive equation coastal ocean circulation model. It solves momentum, continuity, temperature, salinity and density equations on a triangular grid using terrain following co-ordinates in the vertical. FVCOM was implemented over the delta extending from beyond the shelf-break in the Bay of Bengal at the south, to the limit of tidal movement in the north. The model is forced with hourly water levels and daily temperature and salinity at the ocean boundary provided by the GCOMS model [*Kay et al.*, 2015]. River discharge is applied as an upstream boundary; a volume of freshwater is introduced to the model at a single grid point at the northern boundary of the model. The daily discharge volume rate comes from INCA [*Whitehead et al.*, 2015]. Meteorological forcing representing evaporation and precipitation from the delta is not applied locally. The tidal and fluvial hydrodynamics were validated against water level observations and tidal constituent analysis [*Bricheno et al.*, 2016]. River salinity was calibrated against observations made by *Jahan et al.* [2015]. See Table S3 for details on the FVCOM simulated scenarios.

2.3 Linear emulators of hydrological, hydrodynamic and ground water simulations

Daily river elevation and river salinity at 105 locations within the study zone were emulated using the simulation results from Delft3D and FVCOM, respectively. For the ESPA Deltas project [*Nicholls et al.*, 2016], Delft3D and FVCOM were run for several full hydrological years using different socio-economic scenarios and different climate, sea level and upstream river boundary conditions. The results used for the projected soil salinity by 2050 in this study are limited to the scenarios run for the Business As Usual scenario (BAU). BAU is

456 defined as the situation that might exist if existing policies continue and development trajectories
457 proceed along similar lines to the previous 30 years [*Allan and Barbour*, 2016].

458 In this study, we used the Partial Least Square Regression (PLS) to build a set of linear
459 emulators of river elevation and salinity at the 105 virtual river locations and ground water depth
460 and salinity at each one of the 653 unions. Partial least squares (PLS) regression is a technique
461 that combines the principal component analysis (PCA) with the multiple linear regression [*Clark*,
462 1975]. Its goal is to predict a set of dependent variables from a set of independent variables or
463 predictors. This prediction is achieved by extracting from the predictors a set of orthogonal
464 factors called latent variables which have the best predictive power. PLS regression is
465 particularly useful when we need to predict a set of dependent variables from a (very) large set of
466 independent variables (i.e., predictors). Since the dimension of the emulators outputs for this
467 study are large, being 105 for the river elevation and salinity emulators and 653 (i.e. one for each
468 union) for ground water depth and salinity and inundation depth emulators, we used the PCA as
469 a pre-processing technique to reduce the number of output dimensions (See supplementary
470 information text S1 for a more detail description on emulators).

471 The emulators' prediction accuracy is evaluated using the root mean-square error
472 (RMSE). To assess the robustness of the emulators, different percentages of available simulation
473 data set are used to train the emulators and the remaining data set is use to validate the prediction
474 accuracy. The simulation points used to train the model are randomly selected and the RMSE is
475 calculated for the data set not used for training. This is repeated 30 times to obtain a mean RMSE
476 for each percentage of data used for training.

477

478 **3 Soil salinity observations, weather and crop types in coastal Bangladesh**

479 The outputs of the proposed soil salinity model are compared with observed soil salinity
480 values at village level and for the entire coastal region. We compared the model results against
481 the soil salinity observations reported by *Rahman et al.* [2013] under Aman rice and shrimp
482 farming at village level in Satkhira district, the observations of *Mondal et al.* [2001] at two
483 villages in Khulna district and the mean observed soil salinity spatial distribution at coastal
484 Bangladesh between 2001-2009 reported by the Soil Resource Development institute of
485 Bangladesh (SRDI, 2012). All these studies reported soil salinity and some components of the
486 drivers of soil salinity included in the simulation model, but they are not comprehensive. For
487 example, river elevation was not reported by any of these studies and yet is a key variable
488 driving changes of inundation depth, depth to groundwater and groundwater salinity. As a
489 pragmatic approach, we have used the climatic drivers for the three climate ensembles (Q0, Q8

and Q16) and the BAU socio-economic scenario developed in the ESPA Delta project [*Nicholls et al.*, 2016].

Observed monthly average rainfall and temperature at two stations in Satkhira and Khulna district (see locations on Fig. 2) are obtained from Bangladesh Agricultural Research Council climate data base (http://climate.barcapps.gov.bd/index.php).

The model includes a library of 94 different crops (25 species of fish and shrimps has been also included as crop types) organized in 5 different cropping patterns for each upazilla. A review of observed cropping patterns (i.e. sequence of crops on agriculture fields) were carried out to identify typical crops, their varieties and use in coastal Bangladesh. This work utilised the Soil Survey Reports of Bangladesh and the five most frequent cropping patterns were selected for each upazilla (i.e. sub-district). It is assumed that the cropping patterns are the same in each union within a specific upazilla. The percent area used for each cropping pattern is as observed. If more than one crop was grown in a cropping pattern in the same season, their percentage area is assumed to be equal. Observed cropping patterns of the early 1990s are used for simulation years before the year 2000, whereas observations of 2009-2010 are used as present day cropping patterns from 2000 to 2014. It is assumed that the cropping patterns are going to be the same as the present day in the future. The properties of the observed crops (rooting depth, crop coefficient, evaporation depletion factor, salinity tolerance, etc.) are partially collated from field observations (Bangladesh Agriculture Research Institute, BARI, Bangladesh Rice Research Institute, BRRI, and Department of Agricultural Extension, DAE, datasets), partially based on a model calibration exercise described in *Lazar et al.* [2015]. To anticipate future crop varieties, properties of future crops (potential yield and salinity tolerance) were modified based on information published in 'Agricultural Technology for Southern Region' report [*BARC*, 2013]. However, basic crop properties that affect water uptake and other tolerances (e.g. temperature) in the model were not changed, thus these are irrelevant to this paper.

4 Results

4.1 Linear emulator accuracy

In this section, as an exemplar, only the accuracy of mean river elevation is presented. A detail description of the scenarios used to train the emulators and the accuracy of the linear emulators can be found in the supplementary information (S1 to S2).

The predictors used to emulate the river elevation are the INCA simulated up-stream river discharge rate for each one of the three main rivers, and the maximum, mean and standard deviation of the daily sea elevation [*Whitehead et al.*, 2015]. Figure 5 illustrate the daily variability of inputs used for the 15 scenarios altogether. The daily statistics (max, mean and standard deviation) of sea elevation were used to capture the hourly variability that are embedded into the Delft3D/FVCOM daily aggregated results. Most of variability, 99.5%, of the river

527 elevation can be explained with the first 30 principal components for all the 105 river locations
528 reducing the emulator dimension from 105 to 30.

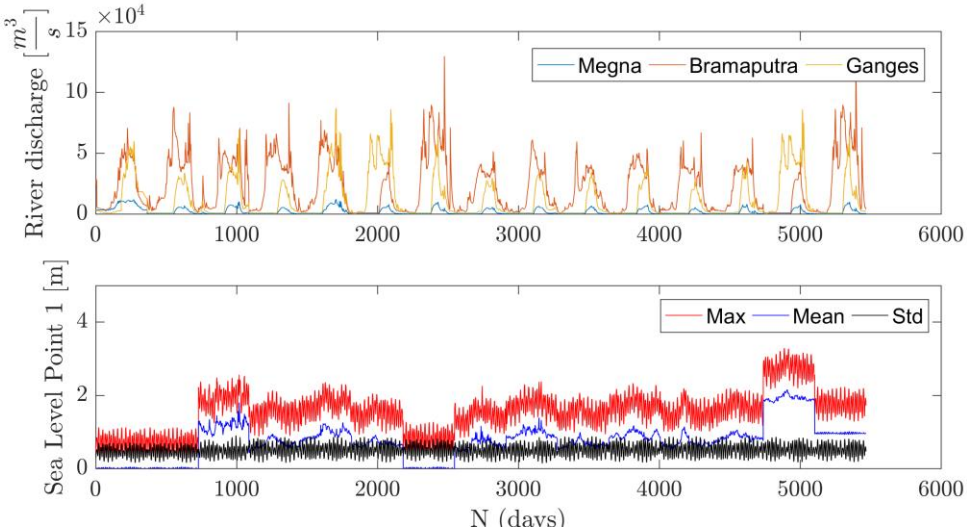

529

530 **Figure 5**. Daily events used to emulate river elevation and river salinity; (a) summarizes the
531 daily upstream river discharge under each of the 15 simulated scenarios for the three main
532 tributaries; and (b) shows the corresponding daily sea level statistics. Daily events are presented
533 as a continuous time series for illustration purposes only (i.e. emulator does not use values of
534 previous day/s to emulate the present day).

535 Linear emulators can accurately reproduce the simulated mean river elevation (Figure 6).
536 The mean *RMS* when only 1% of the data is used is less than 0.4m and this error stabilises
537 around 0.35m when more data is used for training. A detailed investigation of the emulator
538 behaviour reveals that the scenario #14 (i.e. the most extreme temperature and sea level scenario)
539 is the one that consistently produces the largest RMS. Emulated mean river elevation are well

within a factor 10 uncertainty around the target values and are significantly smaller for larger values of water elevation (>~2m) than for smaller river elevation values.

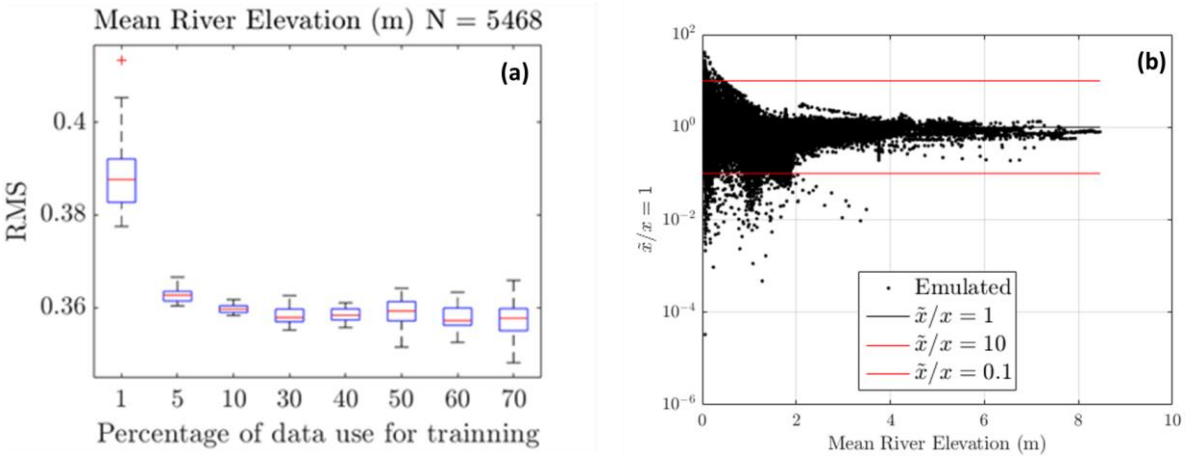

Figure 6. Linear emulators of mean water level in the river: (a) RMS decreases with the percentage of data use for training; and (b) large emulated mean river elevation are well within the uncertainty band of factor ten of simulated values.

4.2 Building confidence on soil salinity model temporal variability

To build confidence on the proposed soil salinity model reproducing the temporal variability of the soil salinity, we have compared the model results against the soil salinity observations reported by *Rahman et al.* [2013] under Aman rice and shrimp farming at village level in Satkhira district and the observations of *Mondal et al.* [2001] at two villages in Khulna district. Both studies reported soil salinity and some components of the drivers of soil salinity included in the simulation model but not all. A comparison between observed temperature and rainfall at Satkhira and Khulna stations against the weather ensembles shows that ensemble Q8 is the closest to the observations, but the daily temperature for the climate ensembles used in soil salinity calculations tends to systematically over-estimate the maximum monthly observed temperatures and under-estimate the lowest temperatures. Rainfall is well within the observed range with some year to year and inter-climate ensembles variability. Because of these differences between model inputs and observed weather conditions, model confidence is assessed against model behaviour relative to the drivers for Q8 ensemble instead that based only on good statistical agreement with observed soil salinities.

The proposed soil salinity model can reproduce the inter-annual variability reported by *Rahman et al.* [2013], but it is very sensitive to the assumed area coverage dedicated to shrimp and rice. *Rahman et al.* [2013] reported the annual maximum and minimum soil salinity values for period 2010-2012 at Shuktia village level under integrated Aman rice and Shrimp farming – traditionally known as Gher. Gher is a modified rice field with high dikes to keep water inside to cultivate shrimps/prawns. This village is within the Khalishkhali union of 38 km^2 of total area,

from which 98% is protected land. The field for cultivating rice in the winter season relies on groundwater irrigation, whereas shrimp are raised in the summer and rainy season using saline water from the nearby Dolua River. Aman rice is cultivated also grown from July to August. The rice variety is not specified thus we have assumed that a high yield variety of Aman rice is grown from July 1st and last 165 days (including nursery and planting) and Bagda is raised on ponds of 0.55m depth and with a water salinity of 12 ppt starting in November 15th for a period of 125 days. The calculated soil salinity for Aman rice shows the expected pattern of soil salinity increase during the dry season followed by salt decrease during the monsoon season (Figure 7). During the rainy season simulated values are consistently lower than reported annual minimum values. Step salinity increases during the Bagda raising period are due to pond recharges to maintain the desired pond water depth. Because *Rahman et al.* [2013] did not reported the area coverage dedicated to shrimp and rice an assumption must be made to be able to compare the model with the observed soil salinity. Two area averaged soil salinity values are calculated: one value assuming shrimp and rice area are equal (i.e. 50% weight for each crop) and other assuming rice area is slightly larger than shrimp area (70% rice and 30% shrimp). The area averaged values during the raising of the crops are in good agreement with the maximum and

585 minimum observed annual soil salinity, being the area averaged values here rice area is dominant
586 in better agreement with observations.

587

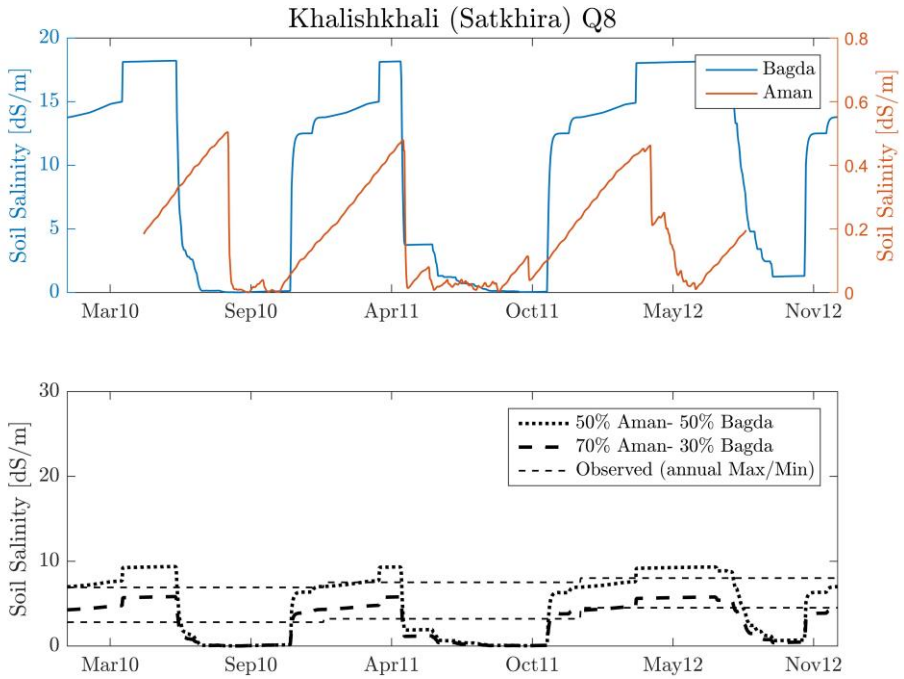

588

589 **Figure 7**. The proposed soil salinity model can reproduce the observed inter-annual variability
590 reported by *Rahman et al.* [2013] for combined Aman rice and Bagda shrimp farming during the
591 period 2010-2012.

592

593 Simulated soil salinity under sesame farming are in good agreement with observed values
594 by *Mondal et al.* [2001] if salt influx from flooding is included. *Mondal et al.* [2001] reported the
595 monthly soil salinity values at two villages (Barondanga and Mirzapur) under non-rice crops for
596 the period 1996-1998. These villages are within the Gutudia Union of 60 km^2 total area, from
597 which 93% is protected land. The field for cultivating non-rice crops (sesame) during the winter
598 season relies on groundwater irrigation. Groundwater at both sites were slightly saline with
599 electrical conductivities from 1.60 to 1.99 dS/m at Barodanga and from 1.75 to 2.04 at Mirzapur.
600 The simulated irrigation water salinity was also saline but with smaller values from 0.49 to 0.88
601 dS/m. For the simulation we assumed that sesame is grown from 15th February during 95 days.
602 Simulated soil salinity under sesame farming in the non-protected area for Q8 ensemble are in
603 better agreement with observed values than the protected land simulations (Figure 8). Observed
604 and simulated soil salinities were much lower during the wet season (July-November) than the
605 dry season (February-May) at both sites. Observed soil salinities at Barodanga varied from 2.25
606 to 12.09 dS/m and from 1.52 to 8.74 at Mirzapur. Simulated soil salinities for the non-protected
607 land varies from 0.82 to 8.54 dS/m for Q8 scenario, from 0.55 to 8.59 dS/m for Q0 scenario and

608 from 1.63 to 11.55 for Q16 scenario. Simulated soil salinities for the protected land were
609 consistently lower than observed values.

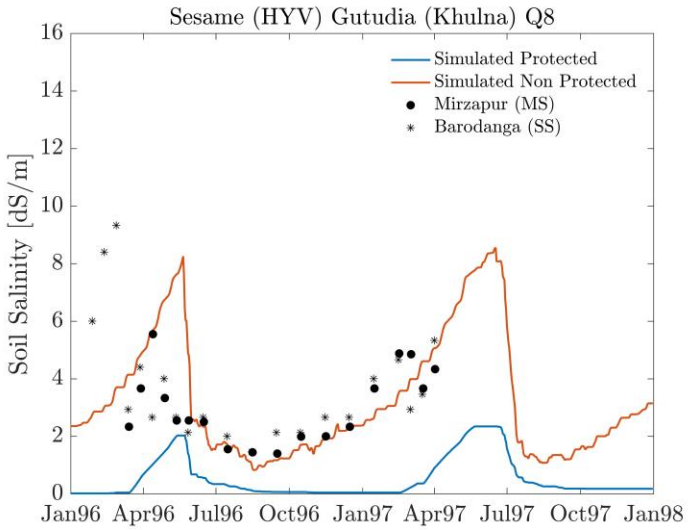

610

611 **Figure 8**. The proposed soil salinity model can reproduce the observed daily variability reported
612 by *Mondal et al.* [2001] for sesame farming during the period 1996-1998 if salt flux from
613 flooding is considered.

614

615 4.3 Building confidence on soil salinity model spatial variability

616 The proposed soil salinity model, for the climate ensemble Q0, can accurately reproduce
617 the observed spatial variability within the weather induced uncertainty. The most comprehensive
618 spatial snap-shot to date on soil salinity in coastal Bangladesh was reported by the Bangladesh
619 Soil Research Development Institute *SRDI* [2010]. The map shown in Figure 9 was created using
620 2500 soil samples of top soils collected during year 2009 and measuring the electrical
621 conductivity of the soil samples from 1:5 soil water extract. The area extent of soils with
622 different degrees of salinity is shown in the map legend as: (1) 31% very slight with salinities
623 from 2.0 to 4.0 dS/m, (2) 26% slight 4.1 to 8.0 dS/m, (3) 18% moderate 8.1 to 12.0 dS/m,
624 (4)15% strong 12.1 to 16.0 dS/m and (5) 10% very strong salinity >16.0 dS/m. The five coloured
625 area types in Figure 9 does not correspond with the five soil salinity degrees but a combination
626 of them as indicated in the map legend making it not straight forward to compare with the union
627 level simulated results. A comparison of the simulated annual median soil salinity with the area
628 extent affected by different degrees of soil salinity suggest that the Q0 ensemble is the closest
629 one to the observations (Table 1). Simulated results for Q0 under estimated the area extent of
630 classes 1 to 4 and over estimate area extent for class 5. Figure 10 shows the observed annual
631 median soil salinity for years 2001 and 2009 as reported by *Dasgupta et al.* [2015] and the
632 simulated soil salinity for the different climate ensembles. Again, the simulated results for

633 climate ensemble Q0 are the closest to the discrete observations. The simulated annual median
634 shows the observed gradient of salinity decreasing with distance from the Sundarbans/coast.

635

636

637

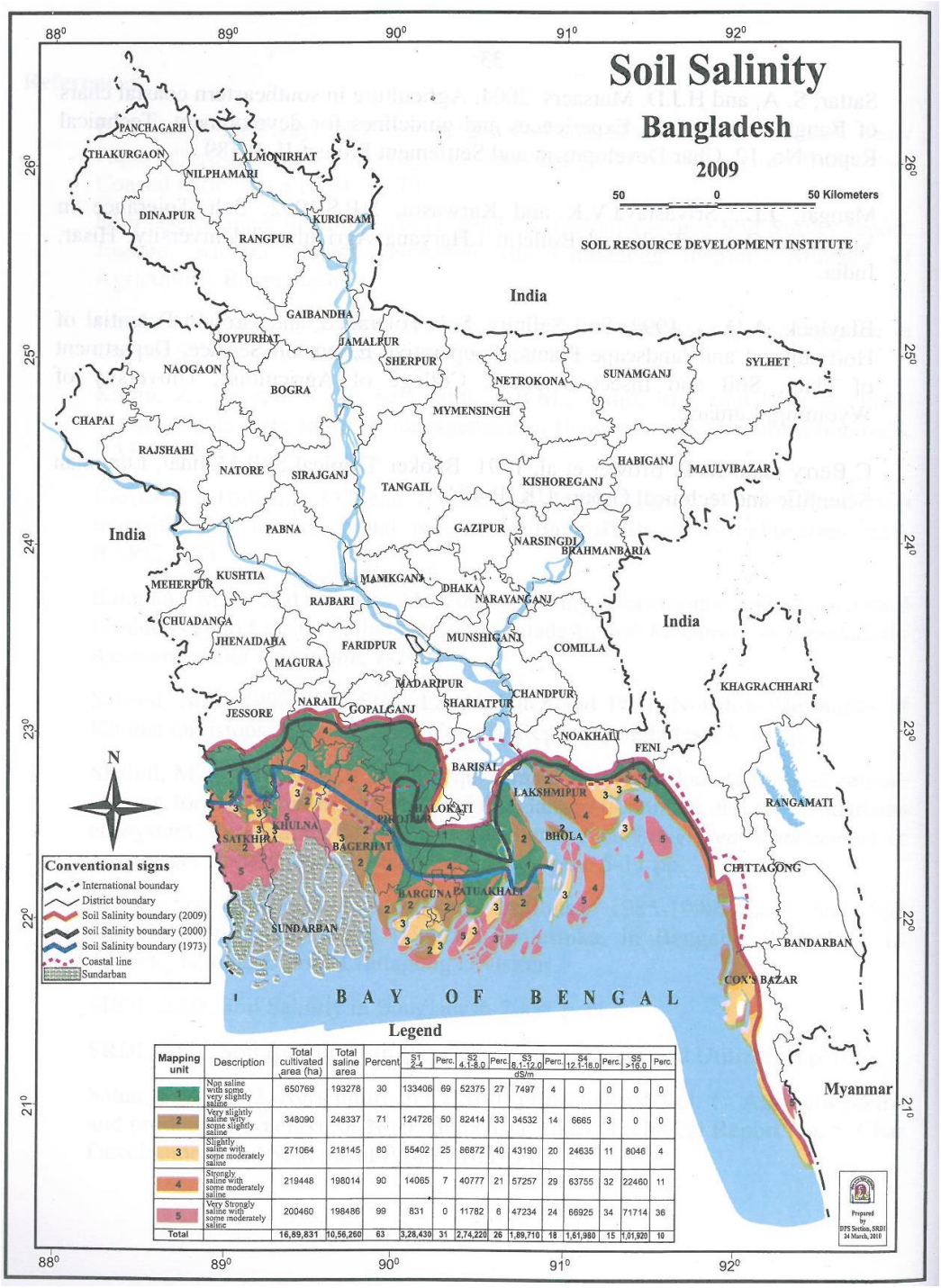

Mapping unit	Description	Total cultivated area (ha)	Total saline area	Percent	S1 2-4	Perc.	S2 4.1-8.0	Perc.	S3 8.1-12.0 dS/m	Perc.	S4 12.1-16.0	Perc.	S5 >16.0	Perc.
1	Non saline with some very slightly saline	650769	193278	30	133406	69	52375	27	7497	4	0	0	0	0
2	Very slightly saline with some slightly saline	348090	248337	71	124726	50	82414	33	34532	14	6665	3	0	0
3	Slightly saline with some moderately saline	271064	218145	80	55402	25	86872	40	43190	20	24635	11	8046	4
4	Strongly saline with some moderately saline	219448	198014	90	14065	7	40777	21	57257	29	63755	32	22460	11
5	Very Strongly saline with some moderately saline	200460	198486	99	831	0	11782	6	47234	24	66925	34	71714	36
Total		16,89,831	10,56,260	63	3,28,430	31	2,74,220	26	1,89,710	18	1,61,980	15	1,01,920	10

638

639 **Figure 9**. Snapshot on year 2009 of spatial variability of soil salinity in coastal Bangladesh
640 (source SRDI, 2010).

641

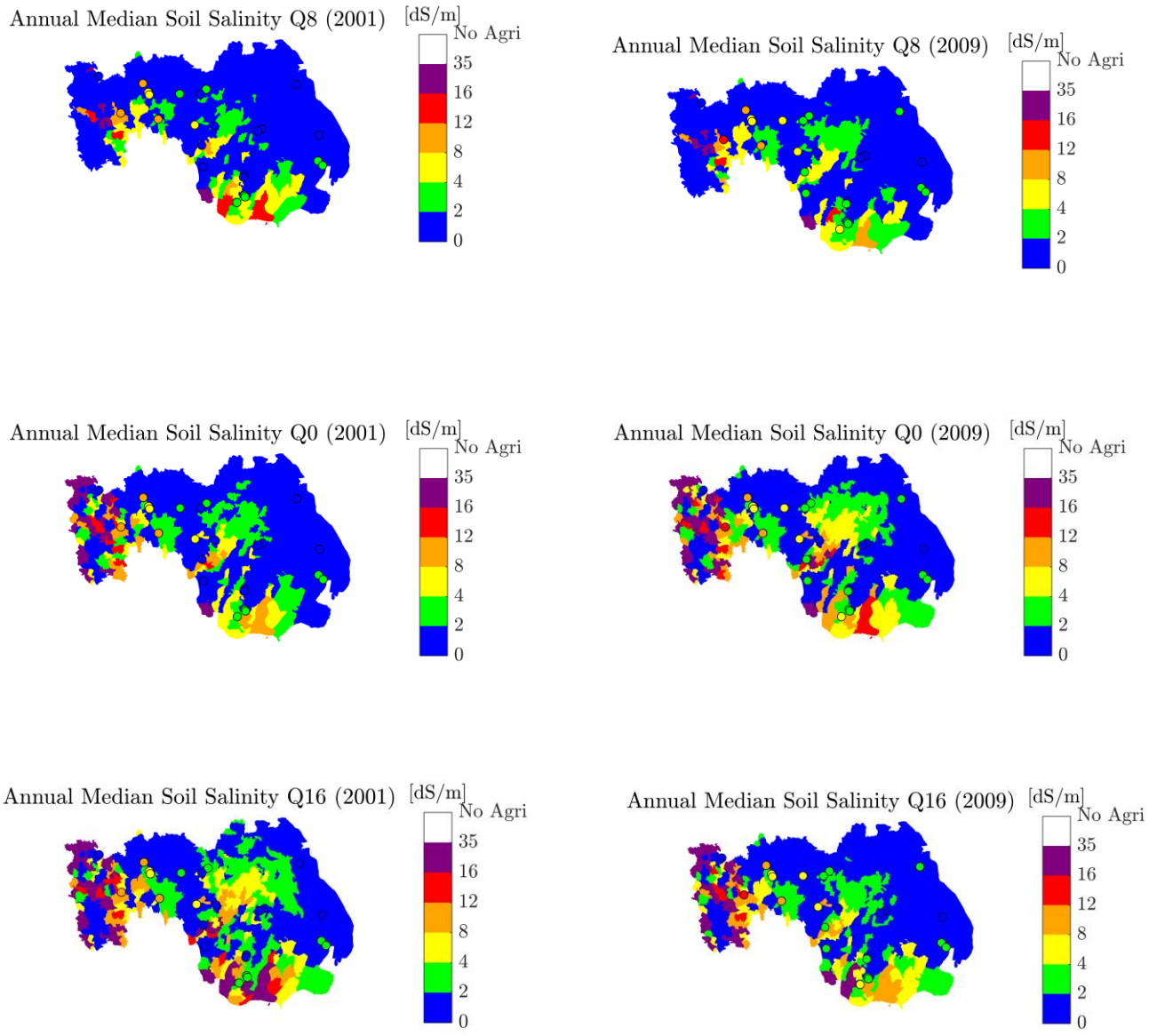

642

643 **Figure 10.** Observed (colored dots) and simulated (colored map) annual median soil salinity for
644 years 2001, 2009 and three climate ensembles. Observations as reported by *Dasgupta et al.*
645 [2015].

646

647 **Table 1.** Extent of soil salinity affected areas observed in year 2009 and simulated annual
648 median for three climate scenarios.
649

Degree of soil salinity	†Extent in (km²)			
	Observed	Q0	Q8	Q16
No saline (<2 dS/m)	6336	8838	12366	10123
Very slight (2-4 dS/m)	3284	3187	2344	2739
Slight (4-8 dS/m)	2742	1969	1319	1442
Moderate (8-12 dS/m)	1897	1038	274	1014
Strong (12-16 dS/m)	1620	487	98	160
Very saline (>16 dS/m)	1019	1106	225	1147

†The river area has been subtracted from the total union area to avoid counting rivers as agriculture land. River area for each union is provided as supplementary information.

650 4.4 Soil salinity projections by 2050

651 Using the proposed simulation model and the three climate scenarios the annual median
652 soil salinity and the maximum soil salinity for the dry season (November to April) and wet
653 season (July-September) for year 2050 has been calculated (Figure 11). The projections obtained
654 by *Dasgupta et al.* [2015] are included for comparison purposes.

655

656

657

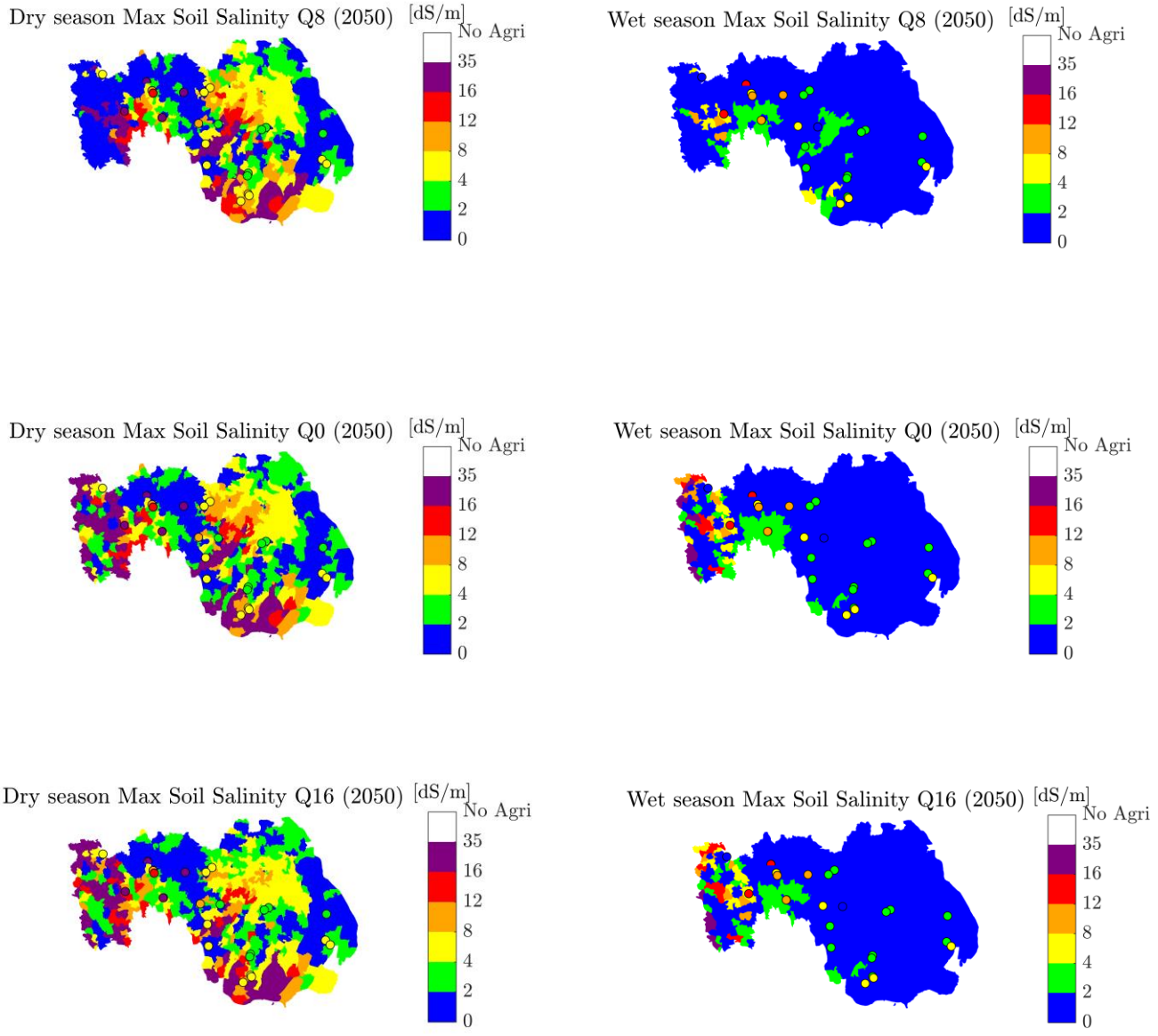

658

659 **Figure 11.** Simulated (colored map) maximum soil salinity for the dry season (November-April)
660 and wet season (July-September) for year 2050 under different climate ensembles. Colored dots
661 represent the estimated soil salinity from Dasgupta et al. [20015].

662
663

664

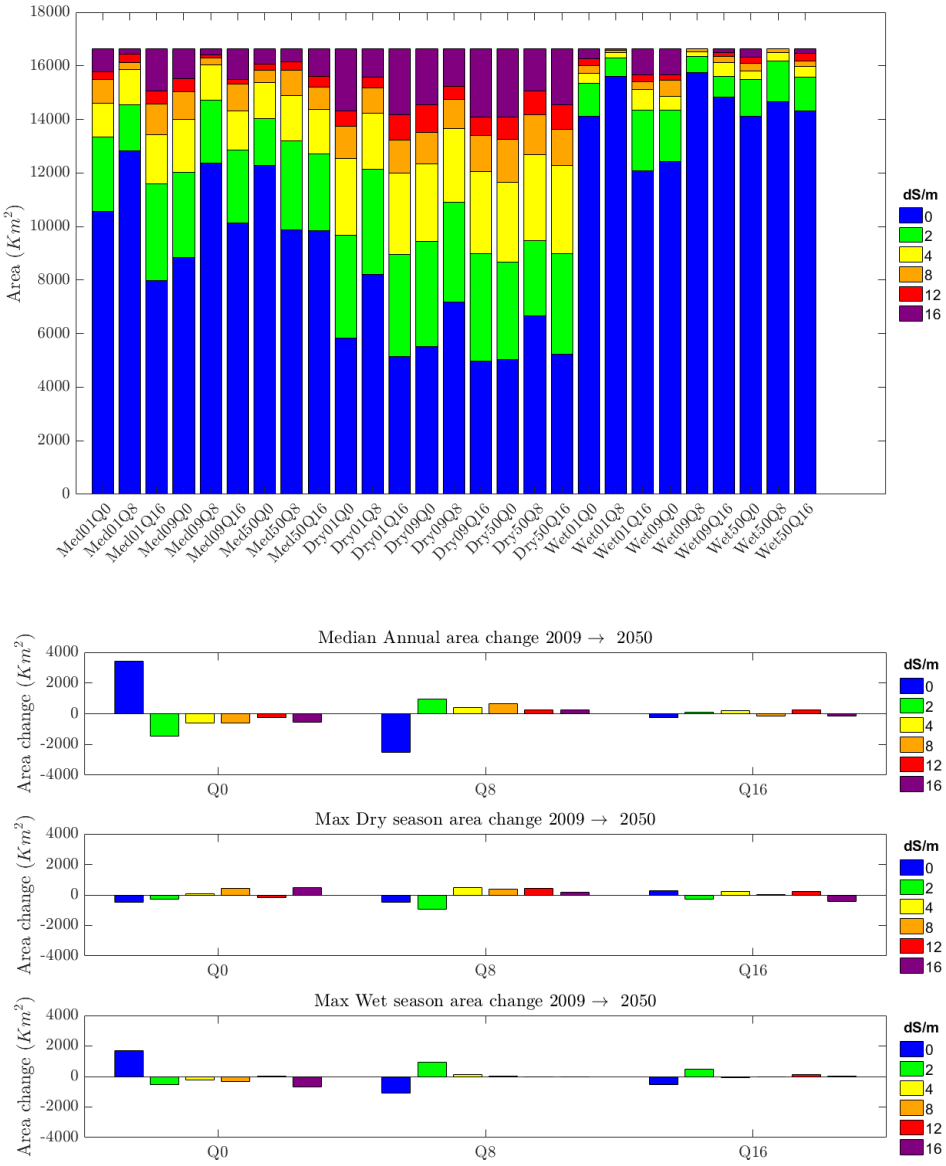

665

666

667 **Figure 12. Simulated area types based on soil salinity degree (top) and relative change of**
668 **median, maximum during dry season and maximum during wet season (bottom) soil**
669 **salinity by 2050. Positive area changes indicate larger area type by 2050 relative to area**
670 **type by 2009.**

671

672 **5 Discussion**

673 We have developed a system dynamic model structure that integrate for first time the key
674 drivers of soil salinity in low lying deltas illustrated in Figure 1 a regional scale. Linear

675 emulators allow us to integrate the different hydrological drivers of soil salinity for the large
676 study area without the large computational time penalty. The time required to emulate all the
677 hydrological variables for all 653 unions for 50-year simulation is ~ 1 minute on a moderately
678 powerful 2015 laptop. The accuracy of the emulated daily hydrological time series is well within
679 a factor ten uncertainty which is considered adequate for modelling purposes and tends to be
680 more accurate for the upper range of values which are often more important (e.g. higher river
681 elevations cause tidal flooding and salt ingress).

682 The approach of using a daily time step and land unit area as proxy for the entire union
683 but divided into protected and non-protected land, seems to capture spatial and temporal
684 variability of soil salinity under different cropping patterns adequately. Dividing the union into
685 protected and non-protected area allows us to obtain a union representative value by area
686 averaging the results. Non protected areas that are prone to flooding, tend to have the largest soil
687 salinity values. The daily time step calculation allows capturing not only the seasonal variability
688 but also the rapid soil salinity wash-out during the monsoon season. We have shown how the
689 model is able to reproduce the seasonal soil salinity increase during the dry season and decrease
690 during the rainy season for integrated rice and shrimp farming and non-rice crops. Using the
691 dominant (e.g. area-wise) cropping pattern for each Union we have shown how the model
692 captures the spatial soil salinity variability for May 2009. The model adequately reproduces the
693 spatial pattern of salinity.

694 Projections by 2050 suggests that the number of unions where soil salinity will increase
695 during the dry season is more numerous than the number of unions where salinity will decrease.
696 Under the Q0 scenario 21% of the unions experience changes in soil salinity larger than 1 dS/m,
697 increasing to 44% under the Q8 and 36% under the Q16 scenarios, respectively. Under Q0 the
698 percentage of unions where soil salinity will increase (11%) is similar to the percentage of
699 unions where it will decrease (10%). Under Q8 and Q16 up to 43% and 32% of unions will
700 increase the dry season soil salinity by at least 1 dS/m, respectively. Clarke et al [2015] indicates
701 that climatic change up to the year 2100 will cause higher temperatures and hence increases in
702 crop evapotranspiration, but the inter-annual variability of rainfall and sequences of dry years
703 was found to be the main driver of increased soil salinity. They also found that in dry years,
704 additional irrigation water can be used, but it will add to the salt load in the agro-soil system.
705 Increased use of dry season irrigation, especially when using water >4dS/m conductivity, will
706 cause the salt balance to pass a tipping point of soil salinity (> 6 dS/m) beyond which crop yields
707 will decline.

708 The proposed method has a number of limitations. The use of emulators to simulate the
709 main hydrological drivers of soil salinity implies that the model is only reliable when the input
710 drivers fall within the range of values used for training the emulators. If any of the simulation
711 data used to train the emulator is biased, the emulator will be also biased. For example, the
712 authors are well aware that the river salinity in the Western region of the study zone are
713 systematically over predicted by the FVCOM simulations. This may be due to missing channels
714 in the delta model such as the Nabaganga river. This channel is not represented in FVCOM, and
715 instead the waters are channelled into the Madhumati (which flows further to the east). There is
716 also the possibility that freshwater sources are missing – as FVCOM is not including
717 evaporation/precipitation. Therefore, soil salinity in this region needs to be interpreted with
718 caution. Our flooding results are realistic, but flooding can change significantly if embankments

719 are breached or elevated. For our flooding simulations we have assumed that flooding occurs
720 without breaching the embankments (i.e. only overtopping occurs). Groundwater pumping is an
721 input to both the simulated and emulated calculations but are imposed as a time varying
722 boundary conditions instead of being dynamically linked to the groundwater stock. Due to the
723 large uncertainty on groundwater stock in coastal Bangladesh [*Richey et al.*, 2015] the authors
724 decided not to attempt in this model version to link groundwater depth to changes in calculated
725 irrigation needs. The modulation of the surface drainage rate by the daily river elevation is an
726 over simplification of the complex daily operation of the polders sluice gates. To effect drainage,
727 gates are opened during low tide to allow drainage, and then closed at high tide to prevent
728 ingress of river water (whether saline or not). Gates are also operated in the dry season to allow
729 inflow of river water for irrigation, provided the river water is fresh. The proposed modulated
730 surface drainage rate is not suited to resolve this active sluice gate operation but to capture the
731 inter daily changes on surface drainage due to changes on the river elevation relative to the
732 polder elevation.

733

734 **6 Conclusions**

735 Understanding the detailed dynamics of salt movement in the soil is a prerequisite for
736 understanding salinity trends and devising appropriate management strategies to improve land
737 productivity of coastal regions. An emulator-based soil salt and water balance at daily time steps
738 provides an additional set of scientifically sound evidence on soil salt dynamic in low lying
739 coastal areas. The proposed approach is demonstrated for the South-West coastal zone of
740 Bangladesh and produces results consistent with the limited observations. Using the proposed
741 approach, we have projected the soil salinity for three different climate ensembles for the period
742 2041-2050, showing potential adverse trends. Using these results, we hope to inform farmers,
743 planners and managers on the likely trajectory of salinity development and the impact of future
744 soil salinity on crop production and on farmers' livelihoods in these sensitive coastal ecosystems.

745

746 **Acknowledgments, Samples, and Data**

747 The authors are grateful to Abdur Razzaque Akanda and Sujit Biswas (Bangladesh
748 Agricultural Research Institute) and Md. Anwarul Abedin and Abu Zofar Md. Moslehuddin
749 (Bangladesh Agriculture University) for providing observed crop properties and cropping
750 patterns, respectively. This work 'Assessing Health, Livelihoods, Ecosystem Services and
751 Poverty Alleviation in Populous Deltas' (NE-J002755-1)' was funded with support from the
752 Ecosystem Services for Poverty Alleviation (ESPA) programme. The ESPA programme is
753 funded by the Department for International Development (DFID), the Economic and Social
754 Research Council (ESRC) and the Natural Environment Research Council (NERC). The support
755 of the UK British Council INSPIRE R-4 programme is appreciated. The authors also
756 acknowledge the use of the IRIDIS High Performance Computing Facility, and associated
757 support services at the University of Southampton, in the completion of this work.

758

References

Allan, A., and E. Barbour (2016), Integrating science, modelling and stakeholders through qualitative and quantitative scenarios, edited, p. 62.

Allen, R. G., L. S. Pereira, D. Raes, and M. Smith (1998), Crop evapotranspiration-Guidelines for computing crop water requirements-FAO Irrigation and drainage paper 56*Rep.*, Food and Agriculture Organization of the United Nations, Rome.

Ayers, R. S., and D. W. Westcot (1985), Water quality for agriculture, FAO Irrigation and Drainage Paper 29*Rep.*, Food and Agriculture Organization of the United Nations, Rome.

BARC (2013), Agricultural Technology for Southern Region of Bangladesh*Rep.*

Bari, M. A., and K. R. J. Smettem (2006), A daily salt balance model for stream salinity generation processes following partial clearing from forest to pasture, *Hydrol. Earth Syst. Sci.*, *10*(4), 519-534, doi:10.5194/hess-10-519-2006.

Barlas, Y. (1996), Formal aspects of model validity and validation in system dynamics, *System dynamics review*, *12*(3), 183-210.

Bricheno, L. M., J. Wolf, and S. Islam (2016), Tidal intrusion within a mega delta: An unstructured grid modelling approach, *Estuarine, Coastal and Shelf Science*, *182*, 12-26.

Caesar, J., T. Janes, A. Lindsay, and B. Bhaskaran (2015), Temperature and precipitation projections over Bangladesh and the upstream Ganges, Brahmaputra and Meghna systems, *Environmental Science: Processes & Impacts*, *17*(6), 1047-1056.

Chen, C., R. C. Beardsley, and G. Cowles (2006), An unstructured grid, finite-volume coastal ocean model: FVCOM user manual, *SMAST/UMASSD*.

Chen, C., H. Liu, and R. C. Beardsley (2003), An unstructured grid, finite-volume, three-dimensional, primitive equations ocean model: application to coastal ocean and estuaries, *Journal of atmospheric and oceanic technology*, *20*(1), 159-186.

Clark, D. (1975), Understanding Canonical Correlation Analysis, in *Concepts and Techniques in Modern Geography, No.3*, edited, Geo Abstracts Ltd, Norwich, UK.

Clarke, D., M. Smith, and K. El-Askari (1998), New software for crop water requirements and irrigation scheduling, *Irrigation and Drainage*, *47*(2), 45-58.

Clarke, D., S. Williams, M. Jahiruddin, K. Parks, and M. Salehin (2015), Projections of on-farm salinity in coastal Bangladesh, *Environmental Science: Processes & Impacts*, *17*(6), 1127-1136, doi:10.1039/C4EM00682H.

Dasgupta, S., M. M. Hossain, M. Huq, and D. Wheeler (2015), Climate change and soil salinity: The case of coastal Bangladesh, *Ambio*, *44*(8), 815-826, doi:10.1007/s13280-015-0681-5.

de Louw, P. G. B., Y. van der Velde, and S. E. A. T. M. van der Zee (2011), Quantifying water and salt fluxes in a lowland polder catchment dominated by boil seepage: a probabilistic end-member mixing approach, *Hydrol. Earth Syst. Sci.*, *15*(7), 2101-2117, doi:10.5194/hess-15-2101-2011.

Deltares (2011), Simulation of multi-dimensional hydrodynamic flows and transport phenomena, including sediments. User Manual of Delft 3D flow*Rep.*, Deltares, The Netharlands.

Doorenbos, J., and W. Pruitt (1977), Irrigation and drainage paper 24, *Crop Water Requirements, FAO, Rome*, 144.

Fatichi, S., and V. Y. Ivanov (2014), Interannual variability of evapotranspiration and vegetation productivity, *Water Resources Research*, *50*(4), 3275-3294.

GED (2009), Policy Study on The Probable Impacts of Climate Change on Poverty and Economic Growth and the Options of Coping with Adverse Effect of Climate Change in Bangladesh, edited, p. 134, General Economics Division, Planning Commission, Government of the People's Republic of Bangladesh & UNDP Bangladesh.

Haque, A., and M. Rahman (2016), Flow Distribution and Sediment Transport Mechanism in the Estuarine Systems of Ganges-Brahmaputra-Meghna Delta, *International Journal of Environmental Science and Development*, *7*(1), 22.

Harbaugh, A. W. (2005), *MODFLOW-2005, the US Geological Survey modular ground-water model: the ground-water flow process*, US Department of the Interior, US Geological Survey Reston, VA, USA.

Hyun, P. S., J. Simm, and H. Ritzema (2009), Development of tidal areas: some principles and issues towards sustainability, *Irrigation and Drainage*, *58*(S1), S52-S59, doi:10.1002/ird.474.

Jahan, M., M. M. A. Chowdhury, M. Shampa, M. Rhaman, and M. A. Hossain (2015), Spatial Variation of Sediment and Some Nutrient Elements in GBM Delta Estuaries: A Preliminary Assessment, paper presented at International Conference on Recent Innovation in Civil Engineering for Sustainable Development (IICSD-2015).

Kay, S., J. Caesar, J. Wolf, L. Bricheno, R. J. Nicholls, A. K. M. Saiful Islam, A. Haque, A. Pardaens, and J. A. Lowe (2015), Modelling the increased frequency of extreme sea levels in the GangesBrahmaputraMeghna delta due

to sea level rise and other effects of climate change, *Environ. Sci.: Processes Impacts*, *17*(7), 1311-1322, doi:10.1039/c4em00683f.
Langevin, C. D., W. B. Shoemaker, and W. Guo (2003), MODFLOW-2000, the US Geological Survey Modular Ground-Water Model--Documentation of the SEAWAT-2000 Version with the Variable-Density Flow Process (VDF) and the Integrated MT3DMS Transport Process (IMT)*Rep. 2331-1258*.
Lazar, A. N., et al. (2015), Agricultural livelihoods in coastal Bangladesh under climate and environmental change a model framework, *Environ. Sci.: Processes Impacts*, *17*(6), 1018-1031, doi:10.1039/c4em00600c.
Mondal, M. K., S. I. Bhuiyan, and D. T. Franco (2001), Soil salinity reduction and prediction of salt dynamics in the coastal ricelands of Bangladesh, *Agricultural Water Management*, *47*(1), 9-23, doi:http://dx.doi.org/10.1016/S0378-3774(00)00098-6.
Muñoz, G., and J. Grieser (2006), Climwat 2.0 for CROPWAT, *Water Resources, Development and Management Service*, 1-5.
Nicholls, R., C. Hutton, A. Lázár, A. Allan, W. Adger, H. Adams, J. Wolf, M. Rahman, and M. Salehin (2016), Integrated assessment of social and environmental sustainability dynamics in the Ganges-Brahmaputra-Meghna delta, Bangladesh, *Estuarine, Coastal and Shelf Science*.
Oosterbaan, R. (2002), SALTMOD; description of principles, user manual, and examples of application.*Rep.*, International Institute for Land Reclmatation and I
mprovement, On website www.waterlog.info/saltmod.htm.
Rahman, M. R., K. Ando, and S. Takeda (2013), *Effect of Shrimp-Based Cropping Systems on Salinity and Soil Fertility in a Coastal Area of Bangladesh: A Village-Level Study*.
Rhoades, J., and S. Merrill (1975), *Assessing the suitability of water for irrigation: theoretical and empirical approaches*, US Department of Agriculture, Agricultural Research Service.
Richey, A. S., B. F. Thomas, M. H. Lo, J. S. Famiglietti, S. Swenson, and M. Rodell (2015), Uncertainty in global groundwater storage estimates in a total groundwater stress framework, *Water resources research*, *51*(7), 5198-5216.
Ritzema, H. (1994), *Drainage principles and applications*, International Institute for Land Reclamation and Improvement (ILRI).
Roelvink, J. (2011), *A guide to modeling coastal morphology*, World Scientific.
SRDI (2010), Saline Soils of Bangladesh: Soil Resources Development Institute*Rep.*, Soil Resources Development Institute.
Tokmakian, R., P. Challenor, and Y. Andrianakis (2012), On the use of emulators with extreme and highly nonlinear geophysical simulators, *Journal of Atmospheric and Oceanic Technology*, *29*(11), 1704-1715.
Whitehead, P. G., et al. (2015), Dynamic modeling of the Ganga river system: impacts of future climate and socio-economic change on flows and nitrogen fluxes in India and Bangladesh, *Environ. Sci.: Processes Impacts*, *17*(6), 1082-1097, doi:10.1039/c4em00616j.